

Constraining photon-axion oscillations using quasar spectra

Edvard Mörtzell[‡] and Ariel Goobar[§],

Department of Physics, Stockholm University,
S-106 91 Stockholm, Sweden

Abstract. Using quasar spectra from the SDSS survey, we constrain the possibility of photon-axion oscillations as a source of dimming of high redshift objects. Such a process has been suggested as an explanation of the apparent faintness of distant Type Ia supernovae. For most combinations of magnetic field strengths and plasma densities along the line of sight, large beam attenuations in broad band filters would also lead to significant differential attenuation, not observed in the quasar sample. However, this conservative study does not exclude the possibility of ~ 0.1 mag dimming of Type Ia supernovae for average plasma densities $n_e \lesssim 10^{-8} \text{ cm}^{-3}$. NIR and MIR spectroscopic studies of high- z sources may be used put further constrains or provide indirect evidence for the existence of a very light axion.

[‡] edvard@physto.se

[§] ariel@physto.se

1. Introduction

One of the most direct and conceptually simple ways to probe the energy densities of the universe is through the redshift-distance relation. The change in the expansion rate caused by the different energy components can be measured by comparing recession velocities (i.e., redshifts) at different epochs of the universe (i.e., different cosmological distances). Type Ia supernovae (SNe) have proved to be very useful distance indicators since, after proper empirical corrections, they have small intrinsic dispersion and are luminous enough to be observed at very large distances. This method has been used by independent groups to show the existence of a dominant energy component with negative pressure, e.g., a cosmological constant [1, 2, 3]. Future supernova (SN) surveys, like the CFHTLS and Supernova/Acceleration Probe (SNAP) [4, 5] will increase the statistics radically, especially at large redshifts, thus making the minimization and control of different systematic effects crucial in order to be able to take full advantage of the increased statistics.

Concerns have been raised about, e.g., evolution of SN properties, gravitational lensing, dust absorption and photon-axion oscillations.

Brightness evolution of SNe can be studied by, e.g., comparing SN lightcurves and spectra at different redshifts and for different host galaxy types. Studies indicate that SNe have quite similar properties, even when formed in very different environments. Therefore cosmic evolution of SN properties or host galaxy extinction is not believed to affect the conclusion of the universe being dominated by a negative pressure component [6].

Systematic effects from gravitational lensing can be diagnosed by studying the induced asymmetry in the luminosity distribution whereas intergalactic dust absorption can be disclosed and corrected for from observed SN colours and spectrophotometry [7, 8].

Photons oscillating into very light axions may cause distant SNe to appear dimmer [9, 10, 11, 12, 13]. The net effect could be confused with the existence of a dark energy component with a negative equation of state. The presence of a significant component of dark energy has recently been independently inferred from other cosmological tests, most notable from recent WMAP background radiation measurements [14] in combination with limits on the Hubble parameter from the HST Key Project [15] and large scale structure measurements from the 2dFGRS survey [16]. Therefore the proposed photon-axion mixing does not replace the need for dark energy, but its equation of state could be different.

The broad-band luminosity distribution and wavelength dependent attenuation caused by photon-axion oscillations have not been studied in any great detail so far. In this paper we examine to what degree it is possible, despite the complicated wavelength dependence of the effect, to put limits on the magnitude of the attenuation by studying a sample of quasar stellar object (QSO) spectra.

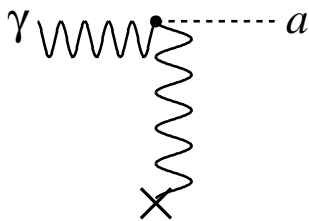


Figure 1. The conversion between photons and axions in an external electromagnetic field.

2. Photon-axion oscillations

Spin 1 particles, as the photon, can mix with zero spin bosons, as the hypothetical axion, in the presence of a mixing agent that allows for the conservation of quantum numbers during the process. The mixing agent could be a magnetic field transverse to the propagation direction of the photon.

The interaction between the photon and the axion is described by the Lagrangian

$$\mathcal{L}_{\text{int}} = \frac{a}{M_a} \vec{E} \cdot \vec{B}, \quad (1)$$

where a is the axion field, M_a is a mass scale determining the strength of the coupling and \vec{E} and \vec{B} are the electrical and magnetic field, respectively. The mass scale is given by

$$M_a \simeq \frac{\pi f_a}{\alpha} \quad (2)$$

where f_a is the decay constant of the axion. Besides the axion decay $a \rightarrow 2\gamma$, this coupling allows for the conversion $a \leftrightarrow \gamma$ in an external electromagnetic field as depicted in Fig. 1.

Due to the interactions with gluons inducing transitions to neutral pion, axions acquire an effective mass, m_a , given by

$$m_a f_a \approx m_\pi f_\pi, \quad (3)$$

where $m_\pi = 135$ MeV is the pion mass and $f_\pi \approx 93$ MeV its decay constant. Note however that the axion mass depends on the quark mass ratios as well as higher-order corrections which are not well known. In this paper, we assume that there exist an axion with $m_a f_a \ll m_\pi f_\pi$.

The most important astrophysical limits on f_a are based on the requirement that the axionic energy loss of, e.g., globular cluster stars or the core of SN1987A, is not too efficient. A lower limit on the decay constant is given by $f_a \gtrsim 10^9$ GeV (corresponding to $m_a \lesssim 10^{-2}$ eV), indicating that axions, if they exist, are very light and very weakly interacting [17].

3. Simulation method

In order to predict the attenuation due to photon oscillations the magnetic field strength configuration and the electron plasma along the line of sight need to be modeled. Earlier work focused on refining the configuration model. However, the tools used to calculate the attenuation were too crude to adequately predict the wavelength dependence of the effect. The most common method used involves a calculation of the attenuation over a very short distance and then these small attenuation elements are added to get results over cosmological distances. Because this method does not treat the oscillatory nature of the interactions, it fails to characterize its differential features along the wavelength axis. A more careful calculation shows that the effect can vary quite fast with wavelength, especially in the optical and IR regime. Thus, the simple approach will introduce errors larger than that caused by the uncertainties in the magnetic field strength and electron plasma density. As demonstrated in Ref. [12], a full density matrix calculation is necessary to get reliable results.

3.1. Magnetic fields and plasma densities

Only model dependent upper limits on the strength of intergalactic magnetic fields are available. This has to do with the fact that the most important observational technique used to trace far-away intergalactic magnetic fields – Faraday rotation – requires knowledge of the intergalactic electron density, n_e as well as the field configurations [18]. The Faraday rotation is the effect of the polarization vector rotating when light travels through a magnetized medium. The polarization vector will rotate by an angle [19]

$$\psi = \frac{e^3}{2\pi m_e^2 c^4} \int_0^l n_e(l) B_{\parallel}(l) \left[\frac{\lambda(l)}{\lambda_{\text{obs}}} \right]^2 dl, \quad (4)$$

where $\lambda(l)$ is the wavelength at position l along the light path. Since neither the intergalactic electron density nor the magnetic field domain size is well known, we have chosen to work with a simple model where the domain sizes correspond to typical galaxy-galaxy separations with an average comoving density, n_e , with a Gaussian dispersion of 50 % between domains. In accordance with Ref. [13], we assume that the magnetic field is frozen into the plasma and subsequently given by $B_0 \propto n_e^{2/3}$ with random direction. For each model, we have tested whether our simulations are consistent with current Faraday rotation measurements. Since the magnetic domains are small compared to the total travel length and the magnetic fields have random directions, the Faraday rotation induced is too small to be used to rule out any of our investigated models.

3.2. Density matrix formalism

The equation to solve for the evolution of the density matrix ρ is given by [20]

$$i\delta_t \rho = \frac{1}{2\omega} [M, \rho], \quad (5)$$

with initial conditions

$$\rho_0 = \begin{pmatrix} \frac{1}{2} & 0 & 0 \\ 0 & \frac{1}{2} & 0 \\ 0 & 0 & 0 \end{pmatrix}. \quad (6)$$

Here the three diagonal elements refer to two different polarization intensities and the axion intensity, respectively and,

$$M = \begin{pmatrix} \Delta_{\perp} & 0 & \Delta_M \cos \alpha \\ 0 & \Delta_{\parallel} & \Delta_M \sin \alpha \\ \Delta_M \cos \alpha & \Delta_M \sin \alpha & \Delta_m \end{pmatrix}. \quad (7)$$

The quantities appearing in this matrix are given by

$$\begin{aligned} \Delta_{\perp} &= -3.6 \times 10^{-25} \left(\frac{\omega}{1 \text{ eV}} \right)^{-1} \left(\frac{n_e}{10^{-8} \text{ cm}^{-3}} \right) \text{ cm}^{-1}, \\ \Delta_{\parallel} &= \Delta_{\perp}, \\ \Delta_M &= 2 \times 10^{-26} \left(\frac{B_{0,\perp}}{10^{-9} \text{ G}} \right) \left(\frac{M_a}{10^{11} \text{ GeV}} \right)^{-1} \text{ cm}^{-1}, \\ \Delta_m &= -2.5 \times 10^{-28} \left(\frac{m_a}{10^{-16} \text{ eV}} \right)^2 \left(\frac{\omega}{1 \text{ eV}} \right)^{-1} \text{ cm}^{-1}, \end{aligned} \quad (8)$$

where $B_{0,\perp}$ is the strength of the magnetic field perpendicular to the direction of the photon, M_a is the inverse coupling between the photon and the axion, n_e is the electron density, m_a is the axion mass and ω is the energy of the photon. The angle α is the angle between a fixed polarization vector and the perpendicular (projected) magnetic field.

We solve the system of 9 coupled (complex) differential equations numerically[†], by following individual light paths through a large number of cells where the strength of the magnetic field and the electron density is determined from predefined distributions and the direction of the magnetic field is random. Through each cell the background cosmology and the wavelength of the photon are updated, as are the matrices ρ and M . In all of our simulations, we use a $[\Omega_M = 0.3, \Omega_{\Lambda} = 0.7, h = 0.7]$ -cosmology. However, the cosmology dependence is quite weak.

3.3. Parameter dependence

In order to study the qualitative behavior of the solutions without any regard to the polarization state of the photons, we rewrite M as a 2×2 matrix,

$$M^{2D} = \begin{pmatrix} \Delta & \Delta_M \\ \Delta_M & \Delta_m \end{pmatrix}, \quad (9)$$

where $\Delta = \Delta_{\perp} = \Delta_{\parallel}$ and Δ_M is the component of the magnetic field parallel to the average polarization vector of the photon beam. We solve Eq. (5) for the density matrix

[†] We have used the `lsoda` package from Netlib, <http://www.netlib.org>

$\rho^{2\text{D}}$ with initial conditions

$$\rho_0 = \begin{pmatrix} 1 & 0 \\ 0 & 0 \end{pmatrix}, \quad (10)$$

where the diagonal elements refer to the photon and the axion intensity respectively. Assuming a homogeneous magnetic field and electron density, we can solve the two-dimensional system analytically. For the $\rho_{11}^{2\text{D}}$ component, referring to the photon intensity, we get

$$\begin{aligned} \rho_{11}^{2\text{D}} &= 1 - \left(\frac{\Delta_{\text{M}}}{2\omega\Omega} \right)^2 (1 - \cos \Omega t), \\ \Omega &= \frac{\sqrt{(\Delta - \Delta_{\text{m}})^2 + 2\Delta_{\text{M}}^2}}{2\omega}. \end{aligned} \quad (11)$$

For values close to the typical set of parameter-values as indicated in Eq. (8), we can set $\Omega \simeq \Delta/(2\omega)$ to get

$$\rho_{11}^{2\text{D}} \simeq 1 - \left(\frac{\Delta_{\text{M}}}{\Delta} \right)^2 (1 - \cos \frac{\Delta t}{2\omega}). \quad (12)$$

The oscillation length is of the order $\sim \text{Mpc}$, i.e., comparable to the size of the domains used in the numerical integration. Note however that this number is very sensitive to the specific input parameter values used. In general smaller magnetic domains (corresponding to smaller cell sizes) yield lower oscillation probabilities, in accordance with the results of Ref. [9].

For $m_{\text{a}} \gg m_{\text{max}} \approx 38\sqrt{n_{\text{e}}/(10^{-8}\text{cm}^{-3})} 10^{-16} \text{ eV}$, the oscillations are suppressed as m_{a}^{-4} . For $m_{\text{a}} \ll m_{\text{max}}$, the effect is quite insensitive to the values of the axion mass which numerical simulations show is true even for $m_{\text{a}} \approx m_{\text{max}}$ [12]. Thus, in all simulations we set $m_{\text{a}} = 10^{-16} \text{ eV}$.

Already from Eq. (8), it is seen that only the combination B_0/M_{a} affects the oscillation probability. Defining $M_{\text{a}}^{11} = \frac{M_{\text{a}}}{10^{11} \text{ GeV}}$, for small mixing angles, the effect is roughly proportional to $(B_0/M_{\text{a}}^{11})^2$ whereas the effect is rather insensitive to the exact value of B_0/M_{a}^{11} in cases of close to maximal mixing. Note that even if the magnetic field strength B_0 would be well constrained from independent measurements, the relevant quantity B_0/M_{a}^{11} will not be, due to our lack of knowledge of M_{a}^{11} .

Generally the effect is stronger for low values of the electron density. The value of n_{e} also has a strong impact on the wavelength dependence of the effect in the respect that higher plasma densities generally cause a more rapid wavelength dependence. In Fig. 2, we show the median QSO spectrum obtained in Ref. [21] unaffected by photon-axion oscillations (upper panel), with $[B_0 = 10^{-9}, n_{\text{e}} \sim 10^{-8}\text{cm}^{-3}]$ (middle panel) and $[B_0 = 10^{-9}, n_{\text{e}} \sim 10^{-9}\text{cm}^{-3}]$ (lower panel) for a redshift of $z = 1$. For $B_0 = 10^{-9} \text{ G}$ and $n_{\text{e}} \sim 10^{-10}\text{cm}^{-3}$, we have an oscillation ‘‘wavelength’’ of $\sim 1000 \text{ \AA}$. For $n_{\text{e}} \sim 10^{-8}\text{cm}^{-3}$, we have variations over an interval of $\sim 10 - 100 \text{ \AA}$ whereas for $n_{\text{e}} \gtrsim 10^{-7}\text{cm}^{-3}$ the variations occur over intervals of $\sim 1 \text{ \AA}$ making them hard to discern from noise.

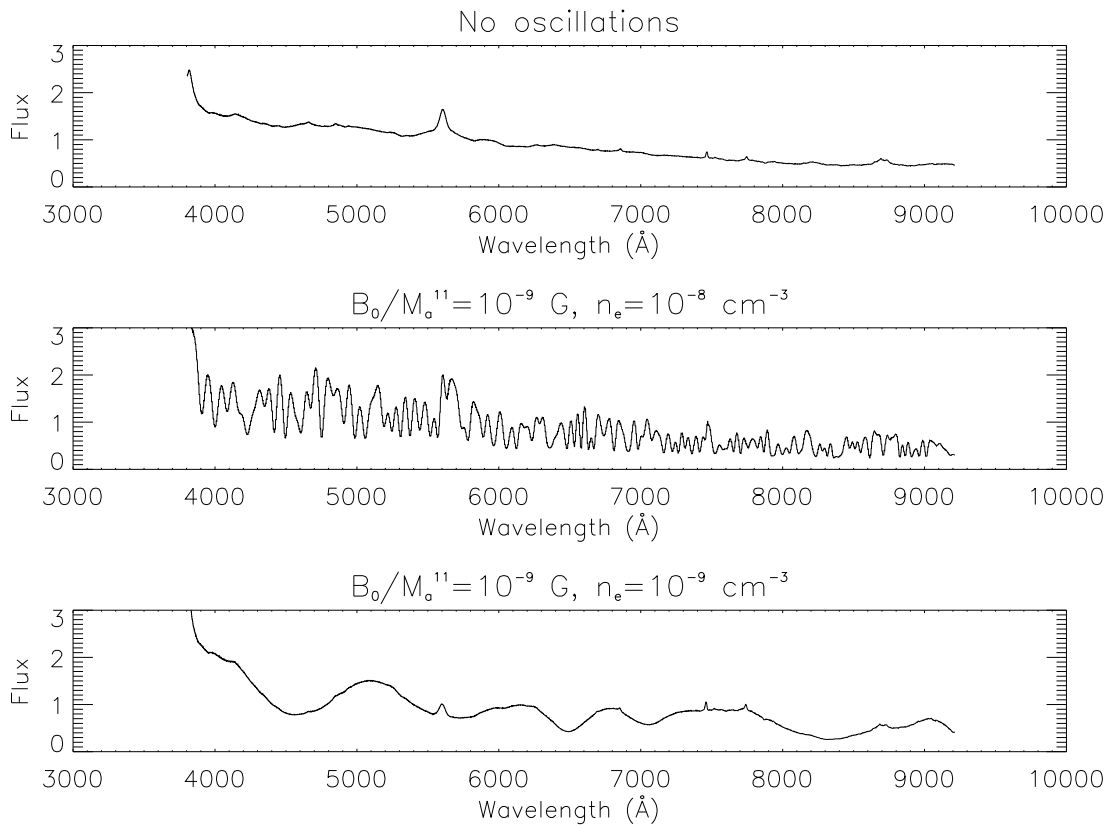


Figure 2. Median QSO spectrum unaffected by photon-axion oscillations (upper panel), with $[B_0 = 10^{-9}, n_e \sim 10^{-8} \text{cm}^{-3}]$ (middle panel) and $[B_0 = 10^{-9}, n_e \sim 10^{-9} \text{cm}^{-3}]$ (lower panel) for a redshift of $z = 1$.

4. Analysis method

One of the main difficulties in constraining photon-axion oscillations is that the effect can look dramatically different for different set of parameter values, as shown in Fig. 2. Given a set of very similar low-noise, high redshift spectra, we should nevertheless be able to put useful constraints on this kind of effect by studying the dispersion around the mean spectrum.

4.1. The sample

We have used a data sample of 3814 QSO spectra from the Sloan Digital Sky Survey (SDSS) Early Data Release (EDR) [22]. The QSOs have redshifts between $z = 0.15$ and 5.03 distributed according to Fig. 3. We divide the QSOs into redshift bins of size $\Delta z = 0.2$ in the interval $0.1 < z < 2.9$. Each spectrum is smoothed by binning the data into wavelengths bins of size 4 \AA (in the restframe) and calculating the mean flux in the data points that fall within each bin. In each redshift bin, we calculate a mean restframe spectrum by normalizing the flux so that we have a mean flux of one (arbitrary units) over the common wavelength interval and average over the smoothed

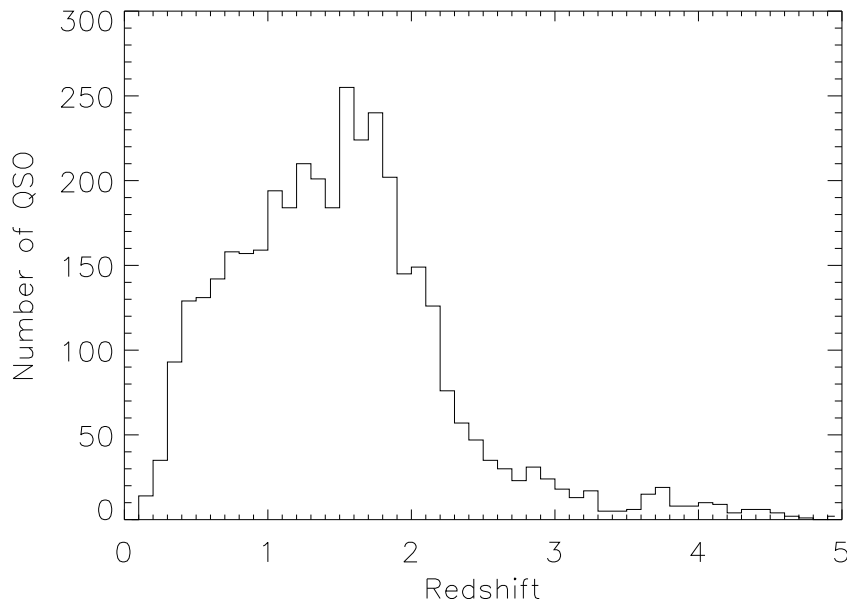


Figure 3. Redshift distribution of 3814 QSO in the Sloan Digital Sky Survey Early Data Release.

spectra. The spectrum-to-spectrum differential variation depends on the wavelength and redshift but is lower than 20 % over large intervals. In Fig. 4, we show the mean spectrum (upper panel) and spectrum-to-spectrum variation (lower panel) in the redshift bin $1.1 < z < 1.3$ consisting of 383 QSOs with a mean redshift of $z = 1.203$.

4.2. Simulated spectra

Using the density matrix method described in Sec. 3.2, we have made a large number of Monte Carlo simulations of the effect on QSO spectra of photons oscillating into axions over cosmological distances. Our parameters are B_0/M_a^{11} and the plasma density n_e . For each set of parameter values and redshift, we add the effect of photon-axion oscillations to the mean spectra derived from the real data set (e.g., for $1.1 < z < 1.3$, upper panel in Fig. 4).

4.3. Statistical analysis

In each redshift bin z , we calculate the dispersion (in flux), $\sigma_{z,i}^r$, around the mean for each spectrum (i). This is done in two steps, where after the first pass, spectral points more than 3 sigma off are rejected not to put excess weight on outliers caused by specific intrinsic features in the spectra. We thus obtain a *distribution* of $\sigma_{z,i}^r$ in each redshift bin, i.e., one number for each spectrum included in the redshift bin. The routine is repeated for the simulated data, with a set of parameters $\vec{\theta} = (B_0/M_a^{11}, n_e)$ giving a corresponding set of $\sigma(\vec{\theta})_{z,i}$. Since photon-axion oscillations only add to the

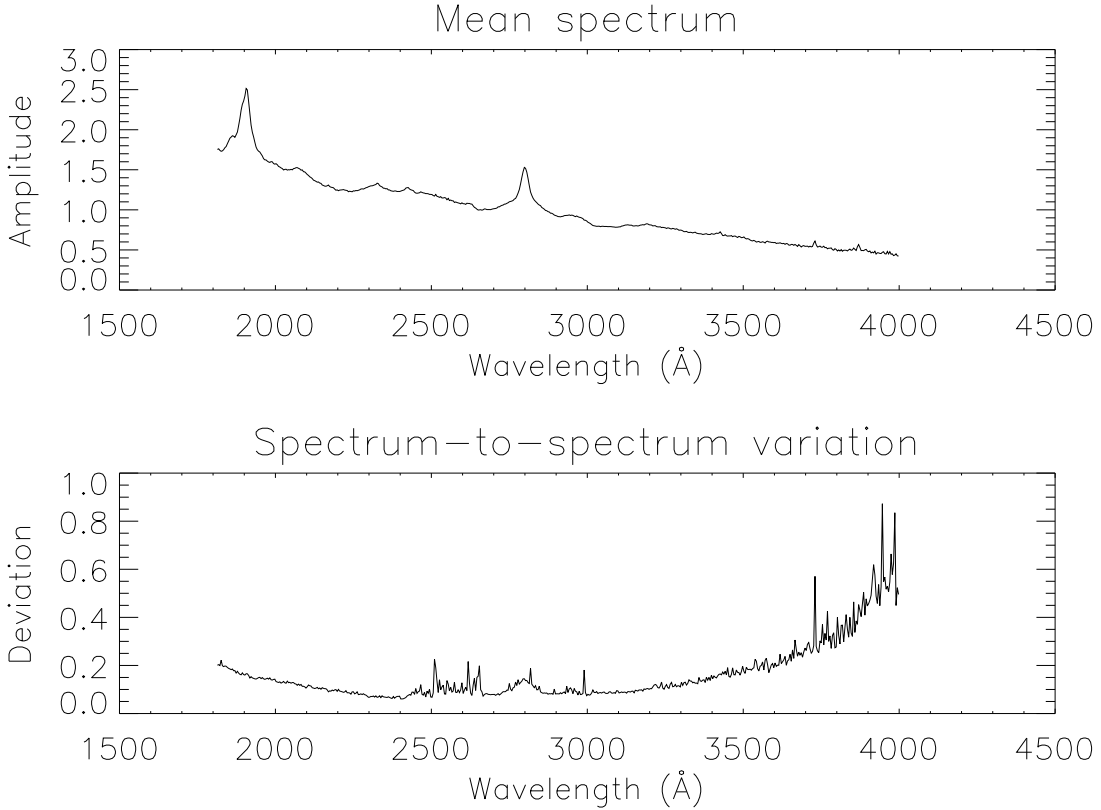


Figure 4. The mean restframe spectrum (upper panel) and spectrum-to-spectrum variation (lower panel) in the redshift bin $1.1 < z < 1.3$ consisting of 383 QSOs with a mean redshift of $z = 1.203$.

intrinsic dispersion, a very conservative approach is to rule out any scenario for which $\sigma_{z,i}^r < \sigma(\vec{\theta})_{z,i}$. Comparing the cumulative distributions $S(\sigma_{z,i}^r)$ and $S(\sigma(\vec{\theta})_{z,i})$ using the Kolmogorov-Smirnov (K-S) test and only taking into consideration the maximum value of the difference $S(\sigma(\vec{\theta})_{z,i}) - S(\sigma_{z,i}^r)$ we can use standard statistics (see, e.g., [23]) to obtain a probability p_z that $\sigma_{z,i}^r$ generally is larger than $\sigma(\vec{\theta})_{z,i}$. By multiplying results from each redshift bin, we obtain a final probability for the configuration vector

$$P(\vec{\theta}) = \prod_z p_z(\vec{\theta}), \quad (13)$$

that $\sigma^r > \sigma(\vec{\theta})$ and can thus rule out a specific set of input parameter values if, e.g., $P(B_0/M_a^{11}, n_e) < 0.05$.

We are also interested in what observational effects each set of parameter values have when integrating over broad band filters. We have investigated this effect by integrating the attenuation over the restframe B-band for Type Ia SNe. In Fig. 5, we have combined the results from this investigation with the results from the K-S test. The grey area indicates the allowed region in the $[B_0/M_a^{11}, n_e]$ -plane from the K-S test using a $P < 0.05$ cut, i.e., roughly corresponding to a 95 % confidence level. Note however that this is a *very* conservative estimation since we have not taken into consideration

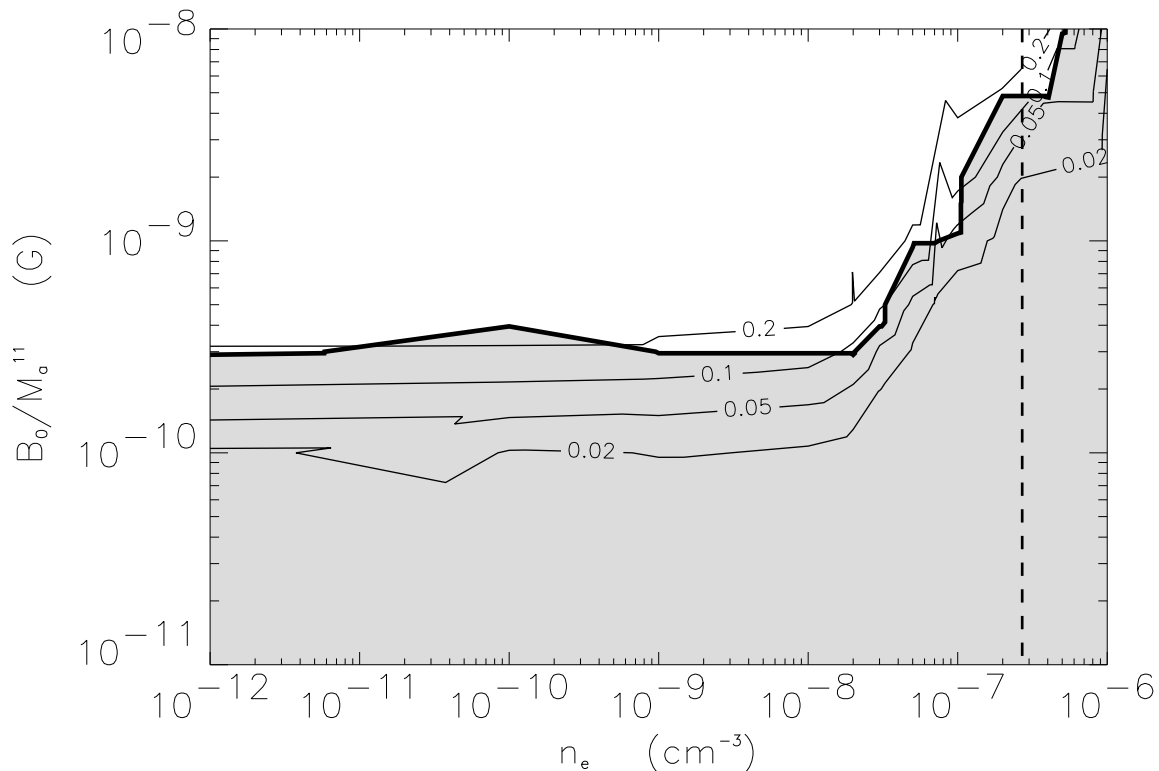


Figure 5. Combined results from restframe B-band attenuation for Type Ia SNe at $z = 0.8$ and the K-S test. Contour levels labeled [0.2,0.1,0.05,0.02] show the amount of attenuation (in magnitudes) while the grey area indicates the 95 % confidence level allowed region from the K-S test. Small scale features are due to low resolution in the parameter grid.

the intrinsic variation of QSO spectra.

The four contour levels labeled [0.2,0.1,0.05,0.02] correspond to the amount of attenuation caused by photon-axion oscillations when integrating over the restframe B-band of a set of Type Ia SNe at a redshift of $z = 0.8$. There is a band in the $[B_0/M_a^{11}, n_e]$ -plane where more than 0.05 mag attenuation results beyond what may be excluded from this analysis. For low values of the plasma density, the allowed attenuation could be as large as 0.2 mag. Also indicated (dashed line) is the baryon density inferred from recent WMAP measurements [14], indicating the maximum allowed value of the plasma density, $n_e \lesssim 2.7 \cdot 10^{-7} \text{ cm}^{-3}$. To test the effect of the data quality on the results, the analysis was also done only including spectra with $S/N > 10$, with a somewhat larger exclusion region as a result, emphasizing the conservative nature of our limits. The small scale features in Fig. 5 are due to low resolution in the parameter grid.

Previous results indicate that low electron densities are required to get an attenuation that increases with redshift. However, since the notion of photon-axion oscillations being solely responsible for the observed faintness of high redshift SNe seems less and less probable when independent cosmological tests support the interpretation

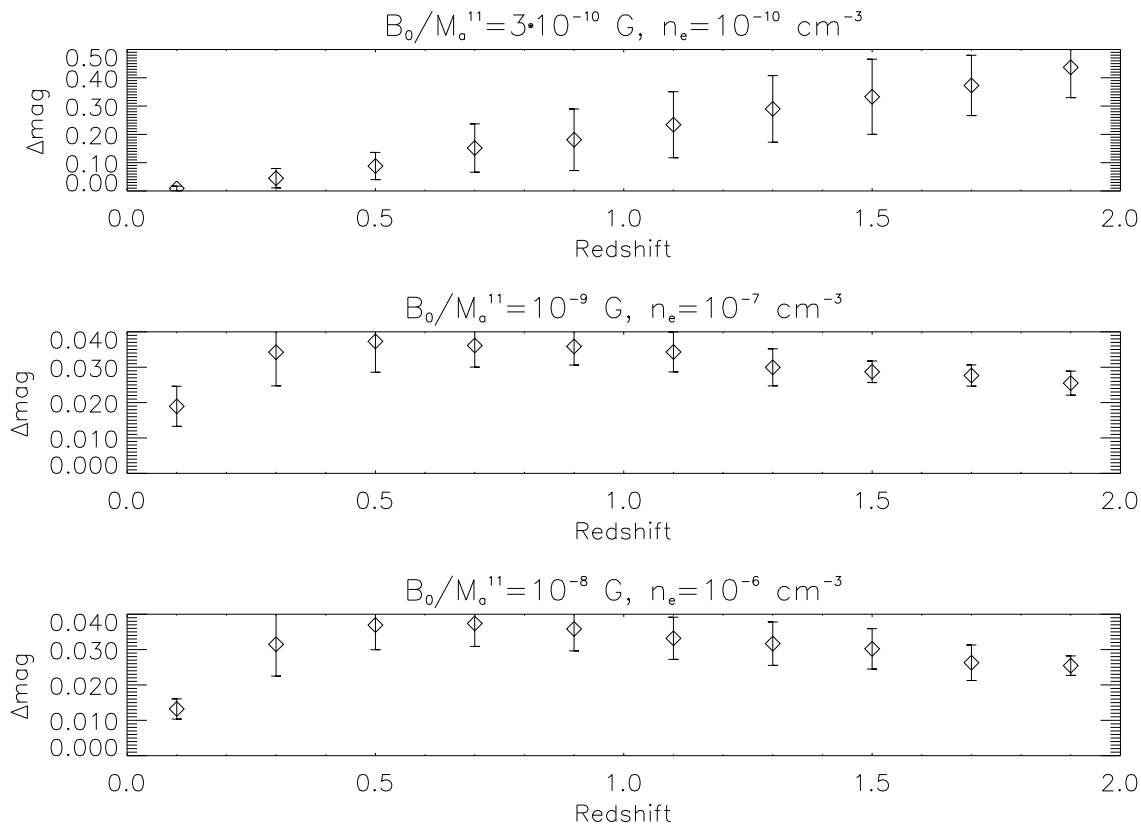


Figure 6. The B-band photon-axion oscillation attenuation integrated over the restframe B-band as function of redshift for $[B_0/M_a^{11} = 3 \cdot 10^{-10} \text{ G}, n_e = 10^{-10} \text{ cm}^{-3}]$ (upper panel), $[B_0/M_a^{11} = 10^{-9} \text{ G}, n_e = 10^{-7} \text{ cm}^{-3}]$ (middle panel) and $[B_0/M_a^{11} = 10^{-8} \text{ G}, n_e = 10^{-6} \text{ cm}^{-3}]$ (lower panel).

of a dominant negative pressure component, we do not restrict our interest to such scenarios. Rather, we are trying to constrain the possible systematic effect for future high precision cosmological tests, e.g., the Supernova/Acceleration Probe (SNAP) [5] aiming at a total error budget of $\Delta\text{mag} < 0.02$. In Fig. 6 we used the SNOC Monte-Carlo simulation package [24] to show the amount of attenuation caused by photon-axion oscillations when integrating over the restframe B-band of a set of Type Ia SNe as a function of redshift for three sets of parameter values passing the K-S test. Note that the result for low plasma densities are very similar to the one for a negative pressure component and that the overall normalization can be set by varying the strength of the magnetic fields and/or the photon-axion coupling strength.

A possible concern is what implications photon-axion oscillations can have for the CMB observations. As noted by previous authors, assuming that the magnetic fields form at relatively low redshifts, the background radiation will be redshifted to such long wavelengths that the effect becomes negligible. This can be seen by studying Eq. (11) for small photon energies. In doing this, we can also see that for infrared (IR) energies, we do have a sizable effect for low plasma densities which can be used to put constraints

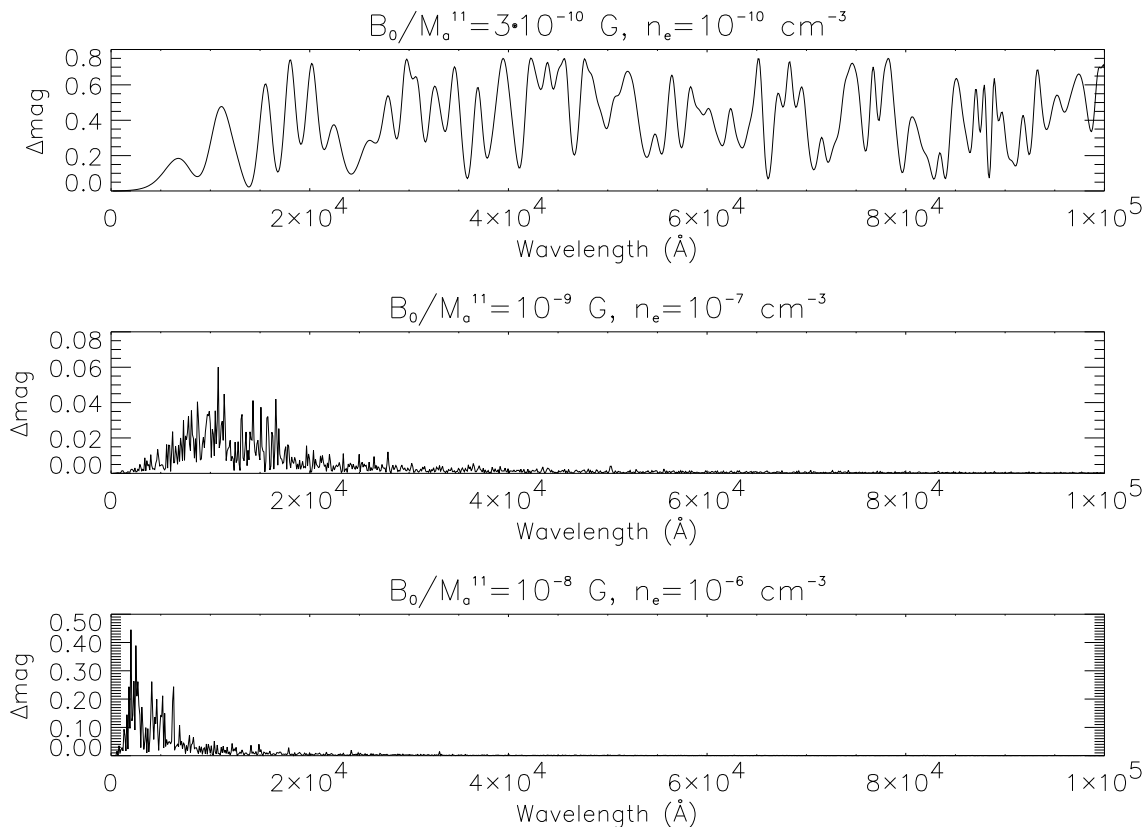


Figure 7. Photon-axion oscillation attenuation over a wide energy range for $[B_0/M_a^{11} = 3 \cdot 10^{-10} \text{ G}, n_e = 10^{-10} \text{ cm}^{-3}]$ (upper panel), $[B_0/M_a^{11} = 10^{-9} \text{ G}, n_e = 10^{-7} \text{ cm}^{-3}]$ (middle panel) and $[B_0/M_a^{11} = 10^{-8} \text{ G}, n_e = 10^{-6} \text{ cm}^{-3}]$ (lower panel).

complementary to what we have derived using only optical spectra, see Fig. 7.

4.4. Polarization

Due to the mixing between the different polarization states and the axion, polarized light might lose some of the polarization when travelling cosmological distances. In contrast to Faraday rotation, this effect can be large even when having a large number of magnetic domains with uncorrelated field strength and direction. Since the amount of depolarization depends on the values of B_0/M_a^{11} and n_e , observations of high redshift polarized sources can be used to put limits on these parameter values. However, the highest degree of polarization observed for high redshift sources is $\sim 20\%$ (see, e.g., Ref. [13] for a short compilation of observations) and by comparing this values with the results depicted in Fig. 8 it is clear that these observations can not be used to add any additional constraints on the magnetic field strength and/or plasma density.

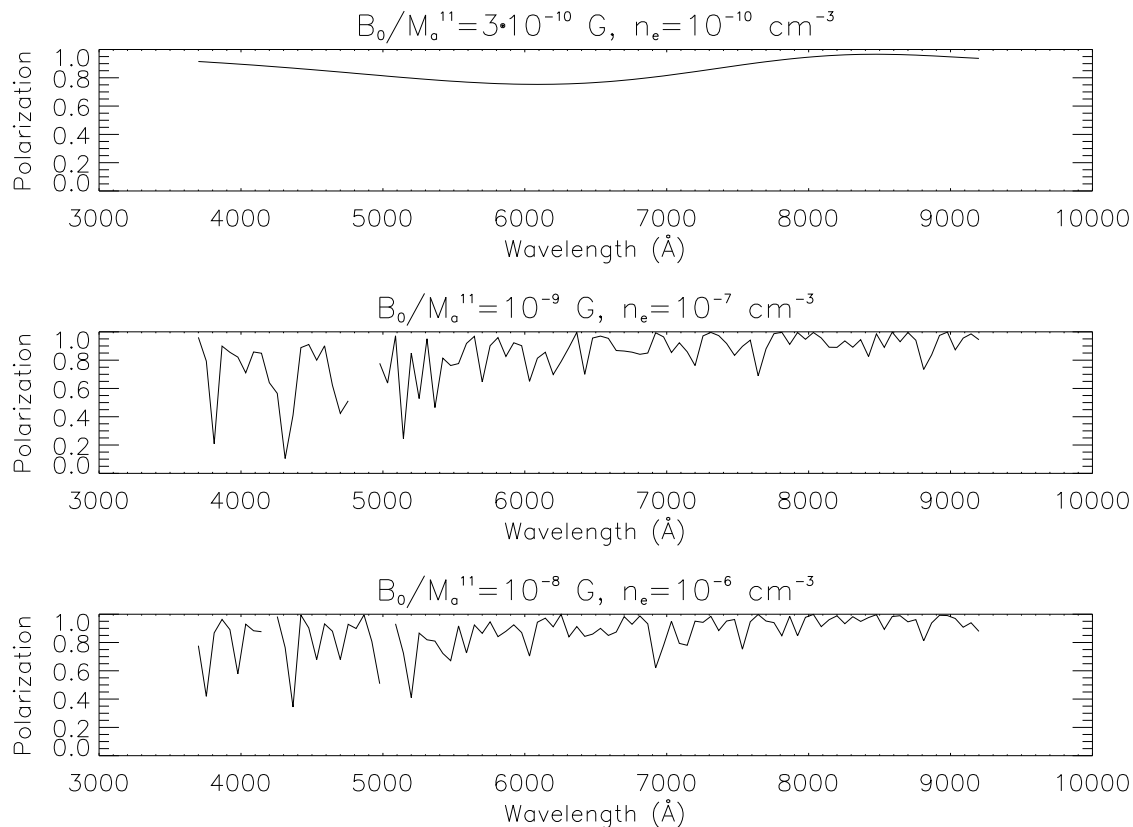


Figure 8. The observed polarization as a function of wavelength for an intrinsically fully polarized source at a redshift of $z = 1$.

5. Discussion

The lack of oscillatory dependence in the differential attenuation of high- z QSO optical light allows us to set severe limits on the parameter space for photon-axion oscillations. However, the present very conservative analysis does not exclude that such effects may be affecting the measured flux of $z \sim 1$ objects at the $\sim 10\%$ level. From Fig. 6, it is clear that assuming a low electron plasma density ($n_e \sim 10^{-10} \text{ cm}^{-3}$), a low mass axion with sufficient coupling strength can imitate the effect of a negative pressure component with respect to the observed luminosity of high redshift sources. Since there are independent cosmological tests supporting the notion of a dominant negative pressure component in the Universe today, such a scenario seems unlikely. However, to ensure the use of, e.g., high- z Type Ia supernovae for precise estimates of cosmological parameters, this issue needs to be addressed further. This could be done by extending our present study of quasar spectra to also include IR information. In the future, instruments like JWST or SNAP may be able to rule out this scenario or provide independent evidence for the existence of a very light axion.

Acknowledgments

The authors would like to thank Georg Raffelt for helpful comments. A.G. is a Royal Swedish Academy Research Fellow supported by a grant from the Knut and Alice Wallenberg Foundation.

- [1] Goobar, A. & Perlmutter, S., 1995, *ApJ*, 450, 14
- [2] Perlmutter, S. *et al.*, *Astrophys. J.*, 517 (1999) 565
- [3] Riess, A. G. *et al.*, *Astron. J.*, 116 (1998) 1009
- [4] Canada-France-Hawaii Telescope Legacy Survey, <http://www.cfht.hawaii.edu/Science/CFHLS>
- [5] SNAP Science Proposal, available at <http://snap.lbl.gov>
- [6] Sullivan, M. *et al.*, arXiv:astro-ph/0211444
- [7] Amanullah, R., Mörtzell, E. & Goobar, A., accepted for publication in *Astron. & Astrophys.*
- [8] Goobar, A., Bergström, L., & Mörtzell, E., *Astron. & Astrophys.*, 384 (2002) 1
- [9] Csaki, C., Kaloper, N., & Terning, J., *Phys. Rev. Lett.*, 88 (2002) 161302
- [10] Deffayet, C., Harari, D., Uzan, J. P. & Zaldarriaga, M., arXiv:hep-ph/0112118
- [11] Csaki, C., Kaloper, N., & Terning, J., arXiv:hep-ph/0112212
- [12] Mörtzell, E., Bergström, L. & Goobar, A., *Phys. Rev. D*, 66 (2002) 047702
- [13] Christensson, M. & Fairbairn, M., arXiv:astro-ph/0207525
- [14] Spergel, D. N. *et al.*, arXiv:astro-ph/0302209
- [15] Freedman, W. L. *et al.*, *Astrophys. J.*, 553 (2001) 47
- [16] Percival, W. J. *et al.*, *MNRAS*, 327 (2001) 1297
- [17] Raffelt G., *Stars as Laboratories for Fundamental Physics* (The University of Chicago Press, Chicago, 1996)
- [18] Grasso, D. & Rubinstein, H. R., *Phys. Rept.*, 348 (2001) 163 [arXiv:astro-ph/0009061]
- [19] Blasi, P., Burles, S. & Olinto, A. V., *Astrophys. J.*, 514 (1999) L79
- [20] Sakurai, J.J. *Modern Quantum Mechanics* (Addison-Wesley Publishing Company, Reading, 1995)
- [21] Vanden Berk, D.E. *et al.*, *Astron. J.*, 122 (2002) 549
- [22] Stoughton, C. *et al.*, *Astron. J.*, 123 (2002) 485
- [23] Numerical Recipes in Fortran 77, Cambridge University Press (available at <http://lib-www.lanl.gov/numerical/bookpdf.html>)
- [24] Goobar, A., Mörtzell, E., Amanullah, R., Goliath, M., Bergström, L. & Dahlén, T., *A&A* 392 (2002) 757